Pump-depletion dynamics and saturation of stimulated Brillouin scattering in shock ignition relevant experiments

S. Zhang,[1] J. Li,[1] C. M. Krauland,[2] F. N. Beg,[1] S. Muller,[2] W. Theobald,[3] J. Palastro,[3] T. Filkins,[3] D. Turnbull,[3] D. Haberberger,[3] C. Ren,[3,4] R. Betti,[3,4] C. Stoeckl,[3] E. M. Campbell,[3] J. Trela,[5] D. Batani,[5] R. H. H. Scott,[6] and M. S. Wei[2,3,*]

[1]*Department of Mechanical and Aerospace Engineering, University of California San Diego, La Jolla, California 92093, USA*
[2]*Inertial Fusion Technology, General Atomics, San Diego, California 92121, USA*
[3]*Laboratory for Laser Energetics, University of Rochester, Rochester, New York 14623, USA*
[4]*Department of Mechanical Engineering, University of Rochester, Rochester, New York 14623, USA*
[5]*Centre Lasers Intenses et Applications, CELIA, Université de Bordeaux CEA-CNRS, 33405 Talence, France*
[6]*Central Laser Facility, STFC Rutherford Appleton Laboratory, Harwell Oxford, Didcot OX11 0QX, United Kingdom*

(Received 5 September 2019; revised 8 February 2021; accepted 19 May 2021; published 16 June 2021)

As an alternative inertial confinement fusion scheme, shock ignition requires a strong converging shock driven by a high-intensity laser pulse to ignite a precompressed fusion capsule. Understanding nonlinear laser-plasma instabilities is crucial to assess and improve the laser-shock energy coupling. Recent experiments conducted on the OMEGA EP laser facility have demonstrated that such instabilities can ~100% deplete the first 0.5 ns of the high-intensity laser. Analyses of the observed laser-generated blast wave suggest that this pump-depletion starts at ~0.02 critical density and progresses to 0.1–0.2 critical density, which is also confirmed by the time-resolved stimulated Raman backscattering spectra. The pump-depletion dynamics can be explained by the breaking of ion-acoustic waves in stimulated Brillouin scattering. Such pump depletion would inhibit the collisional laser energy absorption but may benefit the generation of hot electrons with moderate temperatures for electron shock ignition [Phys. Rev. Lett. **119**, 195001 (2017)].

DOI: 10.1103/PhysRevE.103.063208

I. INTRODUCTION

Shock ignition (SI) is an alternative inertial confinement fusion (ICF) scheme [1,2]. SI utilizes an initial nanosecond pulse at low intensities (10^{14}–10^{15} W/cm^2) to compress a cryogenic DT capsule. Subsequently, a higher-intensity spike (~10^{16} W/cm^2, ~0.5 ns) generates a spherical converging shock to form a nonisobaric hot spot and ignite the compressed fuel [3–7]. The advantage of this scheme is that the separation of compression and ignition phases may provide a more stable implosion and higher energy gain than the conventional central hot-spot ICF [8]. However, the laser-shock energy coupling remains uncertain due to laser-plasma instabilities (LPIs) [9], such as stimulated Raman scattering (SRS), stimulated Brillouin scattering (SBS) [10], and two-plasmon decay (TPD) [11]. Over the duration of the SI spike pulse, all the LPIs are nonlinear and yet to be explored experimentally [12].

Particle-in-cell (PIC) simulations with SI high intensities and large plasma density scale-lengths (L_n = 150–170 μm) have shown >50% SBS reflectivity [13–15], which is not seen in small-scale simulations [16–18] or in experiments [19–26]. Some experiments have observed a burst of SBS at the onset of the laser spike [19,21,22,24]. However, those experiments were limited by either plasma scales (L_n < 170 μm) or low intensities (~10^{14}–10^{15} W/cm^2). The large plasma created by the ignition-scale megajoule (MJ) laser ($L_n \approx$ 300–500 μm and electron temperature $T_e > 3$ keV) can impact the role of each LPI mode [27]. It is also challenging to extend the PIC simulations to full time and spatial scale due to computational limitation. Therefore, experiments are warranted to characterize the LPIs in the interaction between a 10^{16} W/cm^2 laser and a large-scale plasma.

This article reports on a series of experiments to study the laser propagation and LPI physics with SI-relevant intensity (≈10^{16} W/cm^2) in keV plasmas with $L_n \approx$ 260–330 μm, an unexplored regime. We observed strong pump depletion that started at the low-density ($n_e \sim 0.02 n_c$) plasma and progressed into the higher density ($n_e > 0.1 n_c$) region in 0.5 ns. Such nanosecond-scale pump-depletion dynamics can be explained by the local SBS saturation induced by the breaking of the ion-acoustic wave (IAW), which resolves the long-standing discrepancy in the reflectivity data between PIC simulations [13–15] and previous experiments [19–24,26]. These findings have significant implications for the future MJ-scale SI and other high energy density experiments where IAWs with high amplitudes may occur.

II. EXPERIMENTAL SETUP

The experiments were performed on the OMEGA EP laser facility [28] at the Laboratory for Laser Energetics, Rochester, USA. To produce a SI-relevant plasma, one or two UV lasers (2 kJ in 2 ns per beam) irradiated a three-layer disk target (25 μm CH/20 μm Cu/50 μm Al), as shown in Fig. 1.

*mingsheng.wei@rochester.edu

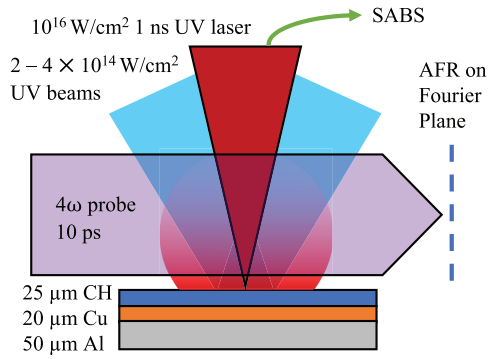

FIG. 1. The experimental setup. One or two 2-ns UV lasers (blue) irradiated the disk target to generate the plasma (light red). One tightly focused 1-ns high-intensity UV laser (red) was injected to interact with the plasma. A 4ω laser (purple) probed the plasma immediately after the laser plasma interaction.

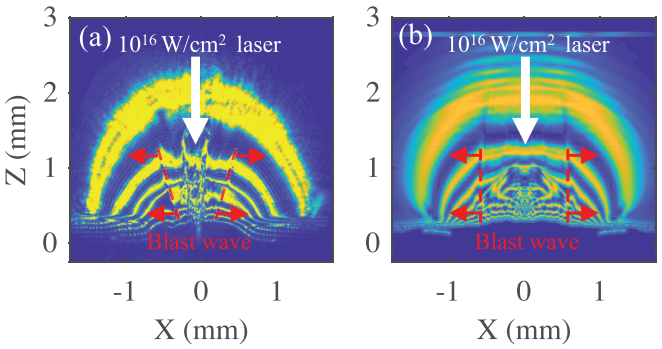

FIG. 2. (a) The experimental AFR image and (b) the FLASH simulated AFR image. The target surface is at $z = 0$. White arrows show the directions of the high-intensity UV interaction lasers driving a blast wave expanding radially. The red dashed lines and arrows mark the blast wavefronts and their moving directions.

The Cu and Al layers were for hot-electron detection [29,30]. The 2-ns UV laser beams had a large smoothed spot using distributed phase plates (750 μm diameter in eighth-order super-Gaussian). Delayed by 1.0–1.5 ns relative to the 2-ns beam onset, a 10^{16} W/cm^2 (1 ns, 1.25 kJ) UV pulse was injected into the plasma along the target-normal direction. The 1-ns beam was focused on the target surface with an 80-μm-diameter spot without a phase plate to maximize the intensity. The laser plasma interaction was characterized by an angular filter refractometry (AFR) using a 10-ps 4ω probe laser ($\lambda = 263$ nm) [31]. The streaked subaperture backscattering spectrometer (SABS) temporally resolved the spectrum of the backward SRS (430–750 nm). A streaked optical pyrometer (SOP) [32] was used to capture the optical emission from the back of the target induced by the shock breakout. The time of the shock breakout is used to infer the total laser energy absorption, which is detailed in the supplemental material [33]. We also used the radiation-hydrodynamic code FLASH [34,35] to simulate the plasma formation and the blast wave generation. FLASH can simulate laser focusing, refraction, and collisional absorption. The simulated plasma formation has been validated in experiments [29,36] and the thermal transport in FLASH is also benchmarked to a NOVA experiment [37].

III. PUMP-DEPLETION MEASUREMENTS

The high-intensity laser generated a conical blast wave expanding radially from the laser axis captured by the AFR measurements. The shapes of the blast waves, shown as the red dashed lines in the AFR images (Fig. 2), indicate that the high-intensity laser is strongly pump-depleted. The blast wave shown in Fig. 2(a) was captured at the end of the interaction laser. The high-intensity laser was delayed by 1.5 ns relative to the start of the low-intensity beam. At the start of the interaction pulse, the plasma has $T_e \approx 1.5$ keV and $L_n \approx 330$ μm in the $n_c/10$–$n_c/4$ region. The blast-wave diameter at the laser entrance, $\phi = 960 \pm 60$ μm at $z = 1.2$ mm ($n_e \sim 0.02n_c$), is 90% larger than the diameter $\phi = 500 \pm 60$ μm at $z = 0.4$ mm ($n_e \sim 0.1n_c$). In contrast with the experiment, in our two-dimensional (2D) FLASH simulation, the high-intensity laser produces a cylindrical blast wave, as shown in the synthetic AFR image in Fig. 2(b). The simulation uses the same $f/6.5$ focusing laser as the experiments. Additional simulations have shown a weak dependence of the blast wave on the laser focusing shape [33]. The simulated and the measured blast waves have similar diameters at the laser entrance ($z = 1.2$ mm) (1.14 mm versus 0.96 mm). However, at $z = 1.0$ to 0.4 mm, the measured blast wave diameters are 20%–60% smaller than those in the simulation. The smaller blast wave at $z < 1.2$ mm indicates the effect of the LPIs, which can cause pump depletion and has not been considered in FLASH simulations.

To understand the cause of the conical blast wave, we evaluated the dependence of the blast wave radius on the LPI-induced pump-depletion by simulating the blast wave driven by a reduced-power laser. These simulations use a laser to heat and penetrate a thin layer of plasma and generate a blast wave propagating in radial direction. Since the plasma is confined by reflective top and bottom boundaries, the simulations are considered as one-dimensional (1D) cylindrical simulations. The initial radial plasma profiles are extracted from the 2D simulations at $z = 0.5$ mm. The laser spot diameter is 200 μm, corresponding to the spot size at $z = 0.5$ mm in the experiments. The laser energy absorption in the thin plasma is calculated by the inverse-bremsstrahlung model, same as the 2D simulations. The radial density profile after the laser interaction is shown in Fig. 3(a). The blast wavefronts are at the steep density gradient, marked by arrows. As shown in Fig. 3(a), the laser power weakly affects the position of the blast wave. When the laser power is reduced by 80%, the blast wave's radial position only decreases by 18% to 430 ± 10 μm (green line), which is still 50% larger than the experimental radius at $z = 0.5$ mm ($r = 290 \pm 30$ μm). Further reducing the laser power to 5% flats the blast wavefront to be unobservable (profile not shown). Thus, the reduced laser power cannot explain the small and clear blast wave observed in the experiment.

In contrast, a delayed laser onset can well reproduce the small blast wave. As shown in Fig. 3(b), when the laser onset is delayed by 0.25 ns (purple line) or 0.50 ns (green)—the first 0.25 ns or 0.50 ns pulse is fully pump depleted and the

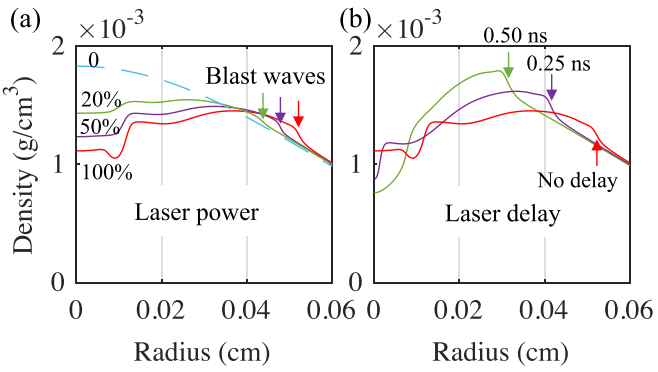

FIG. 3. The density profiles after the laser interaction in 1D simulations 0.5 mm above the target surface. (a) Varied laser power. (b) Delayed laser onset due to strong pump-depletion. The arrows mark the fronts of the blast waves.

remaining 0.75 ns or 0.50 ns pulse has the original power—the simulated blast wave radius decreases linearly from 520 ± 10 μm (r_0 for the no-delay case) to 420 ± 10 or 320 ± 10 μm, respectively. Thus, the relative change $(r_0 - r)/r_0$ of the blast-wave radius is proportional to the pump-depletion time t_{PD} as

$$\frac{r_0 - r}{r_0} = \frac{t_{\mathrm{PD}}}{1.3\ \mathrm{ns}}. \tag{1}$$

This model is also valid in the 1D simulations describing the blast wave at $z = 1.0$ mm with various laser spot sizes (200–300 μm). The weak energy dependence and the linear time dependence suggest that the conical shape of the blast wave can be attributed to a varied pump-depletion time $t_{\mathrm{PD}}(z)$ along the laser axis.

We can calculate the pump-depletion time along the laser axis, $t_{\mathrm{PD}}(z)$, by using the time-dependent blast-wave model (1) and the local ratio of experimental radius to 2D FLASH simulated radius [Fig. 2(b)] as $t_{\mathrm{PD}}(z) = [1 - r_{\mathrm{exp}}(z)/r_{\mathrm{sim}}(z)] \times 1.3$ ns. As shown in Fig. 4, from $z = 1.2$ to 0.4 mm, the

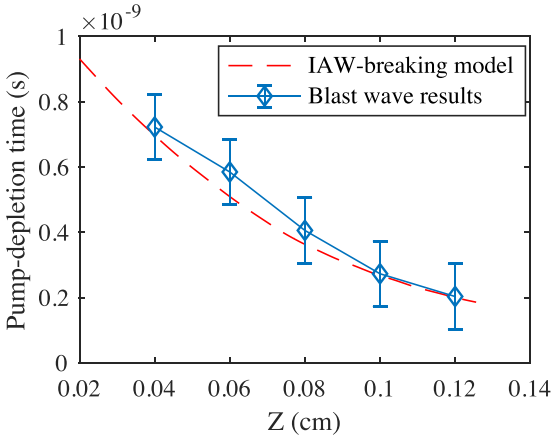

FIG. 4. The pump-depletion times (t_{PD}) in the large-scale underdense plasma at different distances above the target (Z). Blue diamonds are the experimentally inferred t_{PD} from the blast wave analyses. The red dashed line is the t_{PD} curve predicted by the IAW-breaking model.

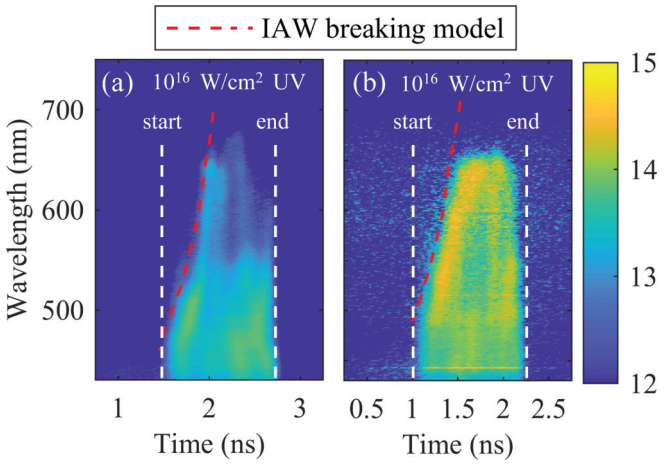

FIG. 5. Streaked SRS spectra from two experiments in different plasma conditions. (a) Same laser and plasma conditions as the blast-wave shot ($L_n \approx 330$ μm, $T_e \approx 1.5$ keV). (b) The plasma has a higher temperature (2.0 keV) and a scale length of 260 μm, and the interaction beam is delayed by 1.0 ns. Time = 0 is the start of the low-intensity UV lasers. The color scale is in $\log_{10}$. Red dashed lines are the pump-depletion positions predicted by the IAW-breaking model.

pump-depletion time t_{PD} increases by 0.5 ns, indicating that the pump-depletion region is moving inward with a speed of $0.005c$. This speed agrees with the prediction from an IAW-breaking SBS saturation model shown as the red dashed line, which is discussed later.

Although the mechanisms other than pump-depletion may affect the laser energy absorption, such as self-focusing and the inhibition of inverse-bremsstrahlung absorption due to the non-Maxwellian distribution, they cannot generate the conical blast wave. Self-focusing is weak in this experiment since the shape of the laser-induced channel in the interaction region as shown in Fig. 2(a) agrees with the theoretical shape of the $f/6.5$ focusing laser. The absorption may be inhibited by a non-Maxwellian distribution; however, this inhibition is equivalent to reducing the laser power, which cannot generate the conical blast wave as discussed above. Laser filamentation and self-focusing, if it occurs, would increase the local intensity and reduce the absorption; however, the increased intensity would enhance SRS, which is against the delayed SRS in the $n_e > 0.05n_c$ region, as discussed below.

Consistent with the blast-wave results, the time-resolved SRS spectra also show strong pump-depletion and a slow laser penetration in the $0.02n_c$–$0.2n_c$ plasma. Figure 5 shows two SRS spectra from experiments in different plasma conditions. The experiment in Fig. 5(a) is under the same conditions as the blast wave experiment. The low-wavelength ($\lambda < 450$ nm) SRS signal from the $n_e < 0.02n_c$ region coincides with the high-intensity laser onset, while the ≈600 nm SRS signal from the $\approx 0.15n_c$ region is delayed by about 0.5 ns. Similar delayed SRS is also observed in the experiment with a higher-temperature plasma, as shown in Fig. 5(b). Note that the absence of SRS from the high-density region during the first 0.5 ns of the high-intensity pulse is contrary to the trend of the SRS convective gain, which increases slightly with the plasma density [38]. This discrepancy indicates that the first

0.5 ns of the laser pulse is depleted in the low-density region, which agrees with the pump-depletion evolution observed in the blast wave.

IV. SATURATION OF STIMULATED BRILLOUIN SCATTERING

Although the mechanism of the pump depletion cannot be directly confirmed in the experiment due to the lack of the full-aperture SBS measurements, our large-scale 2D PIC simulations suggest that nonlinear SBS bursts can grow in the $n_e < 0.05n_c$ region, thereby depleting the laser [38]. On average, only 25% of the laser energy can reach $0.05n_c$. This SBS location agrees with the observed pump depletion at the laser onset. The PIC simulation covered a 900 μm longitudinal length where n_e increased from $0.01n_c$ to $0.28n_c$. However, its 10 ps simulation time is not long enough to show the nanosecond-scale pump-depletion dynamics.

The inward movement of the pump-depletion region along the plasma density gradient can be explained by the IAW-breaking in SBS. An IAW breaks when the ion quiver velocity (v_{quiver}) is close to the wave's phase velocity (c_s), as $v_{\text{quiver}} \approx c_s$ [39,40]. Two IAW modes can grow in a CH plasma: a fast mode dominated by H^+ ions and a slow mode dominated by C^{6+} ions. The phase velocities of each mode (c_{fast} and c_{slow}) are calculated by the kinetic model, expressed as Eq. (20) in Ref. [41], with $T_e(z)$, $T_i(z)$, and $n_e(z)$ from the corresponding FLASH simulations. Under our conditions, $c_{\text{fast}} \sim 1.1\sqrt{T_e/m_H}$ and $c_{\text{slow}} \sim (0.6\text{–}0.8)\sqrt{T_e/m_H}$. v_{quiver} can be calculated from the energy of the IAW (E_{IAW}) since half of the E_{IAW} is the ion kinetic energy and the other half is the potential energy. In the strong SBS case where the laser is fully scattered, the IAW constantly gains energy based on its wave frequency as

$$\frac{dE_{\text{IAW}}}{dt} = \frac{\omega_{cs}}{\omega_0} P_L, \tag{2}$$

where ω_{cs} and ω_0 are the angular frequencies of the IAW and the laser, respectively, and P_L is the laser power. When the light is backscattered, the IAW's wave number k_{IAW} is approximately equal to $2k_L$ to satisfy the momentum conservation [9], so $\omega_{cs}/\omega_0 \approx 2c_s/c$. Accordingly, each IAW mode reaches the breaking condition in a small volume $S_L \Delta z$ when

$$\frac{c_{\text{fast}}}{c} P_L \Delta t \approx \frac{1}{2} N_H m_H c_{\text{fast}}^2 \tag{3}$$

for the fast mode, and

$$\frac{c_{\text{slow}}}{c} P_L \Delta t \approx \frac{1}{2} N_C m_C c_{\text{slow}}^2 \tag{4}$$

for the slow mode, where $N_H = N_C = n_e S_L \Delta z/7$ are the numbers of H^+ and C^{6+} ions in volume $S_L \Delta z$. Here a square pulse with a constant power P_L is assumed, and Δt is each SBS's growing time in the volume and S_L is the laser cross-section at position z. The slow mode saturates ≈8 times slower than the fast mode because of the large mass of the C^{6+} ion, so we only consider the slow mode when calculating the SBS saturation. After all C^{6+} ions in this volume are accelerated to the IAW phase velocity, SBS stops amplifying the IAW and stops reflecting, so the laser can propagate into the next region. The pump-depletion front moves inward with a speed v_{PD} expressed as

$$v_{\text{PD}}(z) = \frac{\Delta z}{\Delta t} \approx \frac{14 P_L}{c_{\text{slow}}(z) n_e(z) S_L(z) c m_C}, \tag{5}$$

in which the laser cross section $S_L(z) = \pi(z/6.5 + 80\ \mu\text{m})^2/4$, corresponding to an $f/6.5$ focusing laser with an 80 μm focal spot at $z = 0$. This model predicts the moving positions of pump depletion, shown as the red dashed lines in Figs. 4 and 5. Although the plasma conditions and the measurement methods are different, the predicted pump-depletion positions in the $0.02n_c$–$0.20n_c$ region agree well with all the experimental results.

V. DISCUSSION

This dynamic pump-depletion has also been observed in small-length-scale PIC or nanosecond-scale hybrid simulations, in which the SBS reflectivity drops to a few percent after a high-reflectivity period [42–45]. References [42,43] discuss a 10^{16} W/cm^2 1-μm laser interacting with a 40-μm-thin $0.3n_c$ H^+ plasma. The SBS reflectivity drops at 6.5 ps after the laser onset. This fast saturation is consistent with Eq. (3), which predicts that IAWs break at 6.2 ps.

The nanosecond-scale dynamic pump depletion can explain why most PIC simulations show stronger SBS than the experiments. The simulations in Refs. [13–15] have millimeter-sized plasmas but the simulation times (<100 ps) are not long enough for the SBS to saturate. According to Eq. (5), the SBS in those simulations would saturate after 500 ps. Reference [17] simulated a smaller (160 μm) D^+ plasma, in which the simulation time (5 ps) is still one order of magnitude shorter than the calculated SBS saturation time. These simulations are still in the SBS growth phase, so the calculated high reflectivity is reasonable. On the other hand, the observed low SBS reflectivity in the previous experiments [19–24,26] could be due to the small plasma scale and the low temperature. Our experiments with a smaller plasma ($L_n \approx 140\ \mu$m) also showed no obvious pump-depletion because the SRS signals from the $n_e > 0.1n_c$ region appeared simultaneously with the interaction laser. Equations (3) and (4) also suggest that the SBS would saturate faster in a low-temperature small-scale plasma. Thus, the measured low SBS reflectivity in previous experiments is consistent with our model.

This strong pump depletion can affect the laser-shock energy coupling in multiple ways. First, the pump depletion can block the laser from reaching the high-density region, reducing the collisional absorption. On the other hand, the pump depletion may benefit electron shock ignition [46–49]. As shown in Fig. 5, the strong pump depletion inhibits TPD, which can produce >100 keV electrons. SRS in the low-density (<$0.2n_c$) region only generates hot electrons with moderate temperature $T_{\text{hot}} < 50$ keV since $T_{\text{hot}} \sim m_e v_{\text{ph}}^2/2$. The measured hot-electron temperature in this experiment is ≈40 keV [30], lower than those in small-scale experiments [19,50] (60–70 keV). This effect favors the electron shock ignition since the low-T_{hot} electrons have been predicted to generate the ignition shock more efficiently [47].

VI. CONCLUSION

In conclusion, the first experiments to characterize LPI at the full-scale SI-relevant laser intensity and plasma conditions have shown evidence of strong pump-depletion of the spike pulse, which is in contrast with previous smaller-scale experiments where SBS was suppressed. The pump depletion was observed to start at the $\sim 0.02 n_c$ low-density region and progress into $0.1 n_c$–$0.2 n_c$ region over the first 0.5 ns of the spike pulse. This dynamic agrees with the IAW-breaking SBS saturation model. The SBS saturation mechanism can explain the reflectivity discrepancy between previous PIC simulations and experiments. The IAW-breaking may further perturb the plasma and impact other LPIs [51], which has not been considered in the SI scheme so far. Furthermore, the strong pump depletion would inhibit the collisional laser absorption in the megajoule-scale SI scheme but may benefit electron shock ignition. Effects of the overlapped beams on LPI and hot-electron generation in SI require further investigation.

ACKNOWLEDGMENTS

We acknowledge the OMEGA EP laser facility staff at the Laboratory for Laser Energetics. This work was performed under the auspices of the U.S. Department of Energy (DOE), National Nuclear Security Administration (NNSA) under the National Laser Users' Facility (NLUF) program with awards number DE-NA0002730 and number DE-NA0003600, and the DOE Office of Science under the High Energy Density Laboratory Plasmas (HEDLP) program with awards number DE-SC0014666 and number DE-SC0012316. The FLASH code used in this work was in part developed by the DOE NNSA-ASC OASCR Flash Center at the University of Chicago. S.Z. thanks Maylis Dozieres, Adam Higginson, and Krish Bhutwala for editing the paper. The support of the DOE does not constitute an endorsement by the DOE of the views expressed in this article.

[1] R. Betti, C. D. Zhou, K. S. Anderson, J. L. Perkins, W. Theobald, and A. A. Solodov, Phys. Rev. Lett. **98**, 155001 (2007).
[2] R. Betti, W. Theobald, C. D. Zhou, K. S. Anderson, P. W. McKenty, S. Skupsky, D. Shvarts, V. N. Goncharov, J. A. Delettrez, P. B. Radha, T. C. Sangster, C. Stoeckl, and D. D. Meyerhofer, J. Phys.: Conf. Ser. **112**, 022024 (2008).
[3] L. J. Perkins, R. Betti, K. N. LaFortune, and W. H. Williams, Phys. Rev. Lett. **103**, 045004 (2009).
[4] K. S. Anderson, R. Betti, P. W. McKenty, T. J. B. Collins, M. Hohenberger, W. Theobald, R. S. Craxton, J. A. Delettrez, M. Lafon, J. A. Marozas, R. Nora, S. Skupsky, and A. Shvydky, Phys. Plasmas **20**, 056312 (2013).
[5] B. Canaud and M. Temporal, New J. Phys. **12**, 043037 (2010).
[6] X. Ribeyre, M. Lafon, G. Schurtz, M. Olazabal-Loumé, J. Breil, S. Galera, and S. Weber, Plasma Phys. Control. Fusion **51**, 124030 (2009).
[7] X. Ribeyre, G. Schurtz, M. Lafon, S. Galera, and S. Weber, Plasma Phys. Control. Fusion **51**, 015013 (2009).
[8] S. Atzeni, X. Ribeyre, G. Schurtz, A. Schmitt, B. Canaud, R. Betti, and L. Perkins, Nucl. Fusion **54**, 054008 (2014).
[9] W. L. Kruer, *The Physics of Laser Plasma Interactions*, Frontiers in Physics (Westview Press, Boulder, Colorado, 2003).
[10] C. S. Liu, M. N. Rosenbluth, and R. B. White, Phys. Fluids **17**, 1211 (1974).
[11] A. Simon, R. W. Short, E. A. Williams, and T. Dewandre, Phys. Fluids **26**, 3107 (1983).
[12] D. Batani, S. Baton, A. Casner, S. Depierreux, M. Hohenberger, O. Klimo, M. Koenig, C. Labaune, X. Ribeyre, C. Rousseaux, G. Schurtz, W. Theobald, and V. Tikhonchuk, Nucl. Fusion **54**, 054009 (2014).
[13] O. Klimo, V. T. Tikhonchuk, X. Ribeyre, G. Schurtz, C. Riconda, S. Weber, and J. Limpouch, Phys. Plasmas **18**, 082709 (2011).
[14] O. Klimo and V. T. Tikhonchuk, Plasma Phys. Control. Fusion **55**, 095002 (2013).
[15] L. Hao, J. Li, W. D. Liu, R. Yan, and C. Ren, Phys. Plasmas **23**, 042702 (2016).
[16] S. Weber and C. Riconda, High Power Laser Sci. Eng. **3**, E6 (2015).
[17] C. Riconda, S. Weber, V. T. Tikhonchuk, and A. Héron, Phys. Plasmas **18**, 092701 (2011).
[18] O. Klimo, J. Psikal, V. T. Tikhonchuk, and S. Weber, Plasma Phys. Control. Fusion **56**, 055010 (2014).
[19] W. Theobald, R. Nora, W. Seka, M. Lafon, K. S. Anderson, M. Hohenberger, F. J. Marshall, D. T. Michel, A. A. Solodov, C. Stoeckl, D. H. Edgell, B. Yaakobi, A. Casner, C. Reverdin, X. Ribeyre, A. Shvydky, A. Vallet, J. Peebles, F. N. Beg, M. S. Wei, and R. Betti, Phys. Plasmas **22**, 056310 (2015).
[20] W. Theobald, R. Nora, M. Lafon, A. Casner, X. Ribeyre, K. Anderson, R. Betti, J. Delettrez, J. Frenje, V. Y. Glebov *et al.*, Phys. Plasmas **19**, 102706 (2012).
[21] S. Depierreux, D. T. Michel, V. Tassin, P. Loiseau, C. Stenz, and C. Labaune, Phys. Rev. Lett. **103**, 115001 (2009).
[22] S. Depierreux, P. Loiseau, D. T. Michel, V. Tassin, C. Stenz, P.-E. Masson-Laborde, C. Goyon, V. Yahia, and C. Labaune, Phys. Plasmas **19**, 012705 (2012).
[23] S. D. Baton, M. Koenig, E. Brambrink, H. P. Schlenvoigt, C. Rousseaux, G. Debras, S. Laffite, P. Loiseau, F. Philippe, X. Ribeyre, and G. Schurtz, Phys. Rev. Lett. **108**, 195002 (2012).
[24] S. D. Baton, E. Le Bel, S. Brygoo, X. Ribeyre, C. Rousseaux, J. Breil, M. Koenig, D. Batani, and D. Raffestin, Phys. Plasmas **24**, 092708 (2017).
[25] C. Goyon, S. Depierreux, V. Yahia, G. Loisel, C. Baccou, C. Courvoisier, N. G. Borisenko, A. Orekhov, O. Rosmej, and C. Labaune, Phys. Rev. Lett. **111**, 235006 (2013).
[26] G. Cristoforetti, L. Antonelli, S. Atzeni, F. Baffigi, F. Barbato, D. Batani, G. Boutoux, A. Colaitis, J. Dostal, R. Dudzak, L. Juha, P. Koester, A. Marocchino, D. Mancelli, P. Nicolai, O. Renner, J. J. Santos, A. Schiavi, M. M. Skoric, M. Smid, P. Straka, and L. A. Gizzi, Phys. Plasmas **25**, 012702 (2018).
[27] M. J. Rosenberg, A. A. Solodov, J. F. Myatt, W. Seka, P. Michel, M. Hohenberger, R. W. Short, R. Epstein, S. P. Regan, E. M. Campbell, T. Chapman, C. Goyon, J. E. Ralph, M. A. Barrios, J. D. Moody, and J. W. Bates, Phys. Rev. Lett. **120**, 055001 (2018).

[28] L. Waxer, D. Maywar, J. Kelly, T. Kessler, B. Kruschwitz, S. Loucks, R. McCrory, D. Meyerhofer, S. Morse, C. Stoeckl, and J. Zuegel, Opt. Photonics News **16**, 30 (2005).

[29] S. Zhang, C. M. Krauland, J. Peebles, J. Li, F. N. Beg, N. Alexander, W. Theobald, R. Betti, D. Haberberger, E. M. Campbell, R. Yan, E. Borwick, C. Ren, and M. S. Wei, Phys. Plasmas **27**, 023111 (2020).

[30] S. Zhang, C. M. Krauland, J. Li, J. Peebles, F. N. Beg, S. Muller, N. Alexander, C. Ren, W. Theobald, R. Betti, D. Haberberger, E. M. Campbell, R. Yan, E. Borwick, J. Trela, D. Batani, P. Nicolai, and M. S. Wei, Generation of collimated moderate temperature electron beam and laser plasma interaction for megajoule shock ignition (unpublished).

[31] D. Haberberger, S. Ivancic, S. X. Hu, R. Boni, M. Barczys, R. S. Craxton, and D. H. Froula, Phys. Plasmas **21**, 056304 (2014).

[32] J. E. Miller, T. R. Boehly, A. Melchior, D. D. Meyerhofer, P. M. Celliers, J. H. Eggert, D. G. Hicks, C. M. Sorce, J. A. Oertel, and P. M. Emmel, Rev. Sci. Instrum. **78**, 034903 (2007).

[33] See Supplemental Material at http://link.aps.org/supplemental/10.1103/PhysRevE.103.063208 for the result of the SOP measurement and additional FLASH simulations for the blast wave analysis. Supplemental Material includes Refs. [32,52].

[34] B. Fryxell, K. Olson, P. Ricker, F. X. Timmes, M. Zingale, D. Q. Lamb, P. MacNeice, R. Rosner, J. W. Truran, and H. Tufo, Astrophys. J., Suppl. Ser. **131**, 273 (2000).

[35] A. Dubey, K. Antypas, M. K. Ganapathy, L. B. Reid, K. Riley, D. Sheeler, A. Siegel, and K. Weide, Parallel Comput. **35**, 512 (2009).

[36] L. Ceurvorst, A. Savin, N. Ratan, M. F. Kasim, J. Sadler, P. A. Norreys, H. Habara, K. A. Tanaka, S. Zhang, M. S. Wei, S. Ivancic, D. H. Froula, and W. Theobald, Phys. Rev. E **97**, 043208 (2018).

[37] D. S. Montgomery, O. L. Landen, R. P. Drake, K. G. Estabrook, H. A. Baldis, S. H. Batha, K. S. Bradley, and R. J. Procassini, Phys. Rev. Lett. **73**, 2055 (1994).

[38] J. Li, S. Zhang, C. M. Krauland, H. Wen, F. N. Beg, C. Ren, and M. S. Wei, Phys. Rev. E **101**, 033206 (2020).

[39] C. N. Judice, J. F. Decker, and R. A. Stern, Phys. Rev. Lett. **30**, 267 (1973).

[40] B. I. Cohen, B. F. Lasinski, A. B. Langdon, and E. A. Williams, Phys. Plasmas **4**, 956 (1997).

[41] E. A. Williams, R. L. Berger, R. P. Drake, A. M. Rubenchik, B. S. Bauer, D. D. Meyerhofer, A. C. Gaeris, and T. W. Johnston, Phys. Plasmas **2**, 129 (1995).

[42] S. Weber, C. Riconda, and V. T. Tikhonchuk, Phys. Rev. Lett. **94**, 055005 (2005).

[43] S. Weber, C. Riconda, and V. T. Tikhonchuk, Phys. Plasmas **12**, 043101 (2005).

[44] L. Divol, B. I. Cohen, E. A. Williams, A. B. Langdon, and B. F. Lasinski, Phys. Plasmas **10**, 3728 (2003).

[45] W. L. Kruer, E. J. Valeo, and K. G. Estabrook, Phys. Rev. Lett. **35**, 1076 (1975).

[46] S. Gus'kov, X. Ribeyre, M. Touati, J.-L. Feugeas, P. Nicolaï, and V. Tikhonchuk, Phys. Rev. Lett. **109**, 255004 (2012).

[47] E. L. Aisa, X. Ribeyre, S. Gus'kov, P. Nicolaï, and V. T. Tikhonchuk, Phys. Plasmas **22**, 102704 (2015).

[48] E. L. Aisa, X. Ribeyre, S. Y. Gus'kov, and V. T. Tikhonchuk, Phys. Plasmas **23**, 082702 (2016).

[49] W. L. Shang, R. Betti, S. X. Hu, K. Woo, L. Hao, C. Ren, A. R. Christopherson, A. Bose, and W. Theobald, Phys. Rev. Lett. **119**, 195001 (2017).

[50] R. Nora, W. Theobald, R. Betti, F. J. Marshall, D. T. Michel, W. Seka, B. Yaakobi, M. Lafon, C. Stoeckl, J. Delettrez, A. A. Solodov, A. Casner, C. Reverdin, X. Ribeyre, A. Vallet, J. Peebles, F. N. Beg, and M. S. Wei, Phys. Rev. Lett. **114**, 045001 (2015).

[51] J. Li, R. Yan, and C. Ren, Phys. Plasmas **24**, 052705 (2017).

[52] P. Nicolaï, J.-L. Feugeas, T. Nguyen-bui, V. Tikhonchuk, L. Antonelli, D. Batani, and Y. Maheut, Phys. Plasmas **22**, 042705 (2015).